

# The Nature of the Broad–Line–Region in the Radio–Loud AGN 3C390.3

Willem Wamsteker<sup>1,2</sup>, Wang Ting-gui<sup>3</sup>, Norbert Schartel<sup>1,2</sup>, Roberto Vio<sup>4</sup>

<sup>1</sup>ESA IUE Observatory, P.O. BOX 50727, 28080 Madrid, Spain

<sup>2</sup>Affiliated with the Astrophysics Division, Space Sciences Department, ESTEC, the Netherlands.

<sup>3</sup>Center for Astrophysics, University of Science and Technology of China, Hefei, 230026, Anhui, P.R. China

<sup>4</sup>Astronomy Department, University of Padova, Vicolo dell Osservatorio 5, 35122, Padova, Italy.

Accepted 1997 February 5, Received 1996 January 2; in original form 1996 January 2

## ABSTRACT

We present the results of an analysis of the ultraviolet and X–Ray variability of the Broad–Line–Radio Galaxy 3C390.3 over 15 years. The UV continuum of 3C390.3 showed large variations with amplitudes of up to a factor of 10. We find:

- (1) The variations of CIV and  $Ly\alpha$  are highly correlated with the UV continuum, and are delayed with respect to the continuum variations by 50–110 days with the red wing of both CIV and  $Ly\alpha$ , leading the blue wing;
- (2) The CIV/ $Ly\alpha$  ratio is positively correlated with both the continuum flux and UV line strength, a behavior different from other AGNs studied so far;
- (3) The blue sides of the  $Ly\alpha$  and CIV profiles are similar to the blue side of the Balmer lines, while the red sides are different, suggesting a different origin for the red peak in the Balmer lines.

The X–Ray spectra of 3C390.3 observed with ROSAT can be well fitted by a single power-law at Galactic absorption with a spectral slope of  $\alpha = 0.9$ . The overall optical, UV to X–Ray spectrum can also be described by a single power law with  $\alpha_{uvx} = 0.89$ , indicating a very weak or no big blue bump. The unusual behavior of CIV/ $Ly\alpha$  variations might be related to this hard ionizing continuum in 3C390.3.

Our results suggest: (1) The broad CIV and  $Ly\alpha$  emitting gas is infalling towards the central object in 3C390.3; (2) The overall behaviour of the CIV/ $Ly\alpha$  ratio and the absence of a big blue bump, strongly indicate the coexistence of optically thick as well as optically thin BLR clouds; (3) Assuming circular symmetry and predominantly circular motion, the BLR gas is situated at  $83 \pm 25$  lightdays from the central source; (4) Under these assumptions and with the derived circular velocity of  $v_{rot} \simeq 2850 \text{ km s}^{-1}$ , the central mass inside this radius is confined to  $1.3 \cdot 10^8 M_{\odot} < M_{CM} < 4.0 \cdot 10^8 M_{\odot}$ ; (6) Comparing our results with those obtained from VLBI and observations of the Fe  $K\alpha$  line, suggests the association of the BLR with a disk, inclined at  $98 \pm 12$  degrees with respect to the direction of superluminal motion of the radio blobs.

**Key words:** Galaxies: individual: 3C390.3 – Galaxies: Seyfert – Ultraviolet: emission line– Galaxies: X–Ray – Galaxies: radio

## 1 INTRODUCTION

Monitoring emission line and continuum variability has proven to be a powerful method to probe the distribution, as well as the physical and kinematic state of the line-emitting gas surrounding Active Galactic Nuclei (see Peterson, 1993 for a review). The photo-ionized gas responds to the energy input from the continuum source with a delay indicative of the light crossing time for the Broad Line Region (BLR). Campaigns by the AGN Watch collaboration, with a high and even temporal sampling, have been carried out

for a few bright Seyfert galaxies, NGC5548 (Clavel et al., 1991; Peterson et al., 1991, 1992; Stirpe et al., 1993; Korista et al., 1995), NGC4151 (Clavel et al., 1991a; Crenshaw et al., 1994), NGC3783 (Reichert et al., 1994) and Fairall-9 (Rodríguez–Pascual et al., 1997). These campaigns have clearly demonstrated the power of this method. The results are important with respect to the following questions on the nature of the BLR: (1) Does BLR size scale as  $r \propto L^{1/2}$ ? (2) How does the emission line ratio vary with continuum? (3) What is the kinematics of BLR? The answer to the first question seems yes. Up to now, all results for Seyfert

galaxies and quasars are consistent with  $r \propto L^{1/2}$  (Peterson, 1993; Kaspi, 1994). Concerning the second question, the CIV/ $Ly\alpha$  ratio decreased with increasing continuum luminosity in NGC5548, Fairall 9, 3C120 (Clavel, Wamsteker and Glass, 1987; Wamsteker et al., 1990; Gondhalekar, 1992). Three possibilities have been proposed to explain this behavior: a change in the shape of the ionizing continuum (Clavel et al., 1988), optical thin BLR material (Wamsteker & Colina, 1986) or a mixed population of optically thin and thick BLR clouds (Shields et al., 1995). Regarding the kinetics of the BLR, there exists some evidence for infall in Fairall 9 (Recondo et al., 1997; Koratkar & Gaskell, 1991). Accurate determinations of the size of the broad emission line region and, in some cases, the responsive-average geometry (Transfer Function, TF) have been derived from these data (Krolik et al., 1991; Horne et al., 1991; Ferland et al., 1992). While detailed interpretation of the Transfer Function is subtle and to a significant extent model dependent (Maoz, 1994), these analyses show: (1) the broad emission lines respond to the continuum variations very fast and show a dependence on the ionization level of the ions, with the shortest response time for the highest ionization lines (Korista et al., 1995; Peterson, 1993), and (2) the line-emitting gas is not dominated by radial motion. The red wing of CIV has been suggested to lead to the blue wing in NGC5548 (Korista et al., 1995; Wanders et al., 1995), but this result may be a consequence of the blending of CIV with the very broad wings of HeII. However, the general validity of the above results remains still an open question. There are still too few objects for which BLR sizes are 'reasonably' determined and furthermore, all these analyses are limited to the radio quiet objects with big blue bumps and regular emission line profiles. Although observations with high temporal sampling are only available for these four Seyfert I galaxies, one can still use the long term, unevenly sampled, observations with the International Ultraviolet Explorer (IUE) and ground based optical observations to derive estimates of the size and kinematics for other AGNs. Especially for radio galaxies and other galaxies without a big blue bump, where no systematic monitoring has been done, this could be of interest. In this paper, we will present an analysis of the variability of 3C390.3, based on the UV and X-Ray observations made between 1978 and 1992.

3C390.3 (1845+796) is a FR II radio galaxy at redshift  $z=0.0561$ . Superluminal motions were observed at radio wavelengths (Alef et al., 1988). Large amplitude variations have been reported in optical, UV and X-Ray bands (Lloyd, 1984; Veilleux & Zheng, 1991; Clavel & Wamsteker, 1987; Inda et al., 1994). The IUE observations of this object prior to 1986 have been discussed by Clavel & Wamsteker (1987) and variations of the narrow  $Ly\alpha$  and CIV were reported. Also, line variations confined to a restricted velocity range in the broad UV emission lines have been reported by Wamsteker & Clavel (1989). Zheng (1996) discussed independently the UV variability based on the same observational material as used here. The profiles of the Balmer lines are very broad and double peaked (Osterbrock, Koski and Phillips, 1977). Veilleux & Zheng (1991) found that the peak at the blue side of  $H\beta$  followed the variation of the continuum closely and drifted in velocity with time, but the peak at the red side ( $v = 3000 \text{ km s}^{-1}$ ) did not. The double peaked profile and its variations were in-

terpreted to indicate the presence of a relativistic accretion disk (Pérez et al., 1988; Chen & Halpern, 1989) or to suggest biconical outflow (Zheng, Veilleux & Grandi, 1991). From observations with the Ginga satellite a weak  $K\alpha$  emission (6.4 keV) of Fe was found in the X-Ray spectrum of 3C390.3 by Inda et al. (1994) and new observations with ASCA have resolved the line and are discussed by Eracleous et al. (1996). The infrared to optical spectrum is very steep, and no big blue bump appears to be present in this object (Miley et al., 1984). In §2 of this paper, we describe the data and the processing methods. The results are presented in §3. In §4, we discuss the implications of these results. Finally, the conclusions are summarized in §5. Zheng (1996) discussed the same data as we present, the differences between his results and ours are mostly due to the different methods used for the determination of the UV continuum shape and the application of a line model derived from the optical data to the UV lines. We show below that the application of such model to the  $Ly\alpha$  and the CIV line is not justified.

## 2 DATA REDUCTION AND ANALYSIS

A total of 39 short wavelength (SWP: 1150–1980 Å) IUE observations have been taken between 1978 and 1992 (see also Courvoisier and Paltini, 1992). The observation dates and continuum fluxes are listed in Table 1. We used the geometrically and photometrically corrected Extended Line-by-Line (ELBL) files, produced by the IUESIPS reduction, which were cleaned of cosmic-ray hits and other blemishes. The UV spectra were then extracted from the ELBL files by a modified Gaussian extraction (GEX) technique (Reichert et al., 1994) using the routines written at the IUE Data Analysis Center (IUEDAC) and calibrated using the standard IUE sensitivity curve, including the corrections for time and temperature (THDA) sensitivity degradation of the SWP camera. Galactic reddening of  $E(B-V)=0.085$  has been applied to all spectra using the reddening curve of Seaton (1979). To bring all spectra on the same wavelength scale (i.e. correct for centering errors in the IUE Large Aperture), the narrow CIV lines were fitted by a single Gaussian and the central wavelengths were made to coincide at 1635.9 Å.

The continuum measurements in Table 1 are made in two pseudo line-free bands at 1330 – 1370 Å and 1775 – 1825 Å in the rest frame of 3C390.3. The continuum flux is the mean over the bandpass, and the error is the standard deviation of the mean over this bandpass. The continuum at 1800 Å is contaminated by the UV FeII blends lines at the 10% level, as estimated from the mean spectrum (see also below). The continuum level underneath the emission lines was determined by a power-law derived from these two continuum windows.

Veilleux et al. (1990) found that the blue peak of  $H\beta$  extends over the velocity interval of (-7000, 0)  $\text{km s}^{-1}$  relative to systemic velocity. This velocity range corresponds to that in which most of the blue part of CIV is emitted. To maintain the differences reported previously for different velocity domains of the broad lines (Wamsteker & Clavel, 1989), we subdivided both CIV and  $Ly\alpha$  in three parts: the blue-side (-7000 to -1800  $\text{km s}^{-1}$ ); the red-side (1800 to 7000  $\text{km s}^{-1}$ ) and the core (-1800 to +1800  $\text{km s}^{-1}$ ). The red side was chosen in symmetry with the blue side.

More complex fitting techniques, as e.g. applied by Zheng (1996), are not necessarily superior with S/N levels as in the IUE spectra of 3C390.3. Also, the detailed application of the line model derived from the optical data is not valid in this case (see also Figure 5).

Although the overall lightcurves of Zheng (1996) are quite similar to those presented here, we have, in view of the rather different analysis techniques, not made a further detailed comparison with his data and the data in Tables 1 and 2. (N.B. the data in our Table 1 and 2 have been corrected for reddening as above). A comparison of CIV and  $H\beta$  profile (see Figure 5) shows: (1) The blue side of CIV and Balmer line profile is very similar: the peak velocities are the same within the uncertainty; (2) The red sides of profiles are different, Balmer line shows a strong red bump peaked around  $+3000 \text{ km s}^{-1}$ , however, only a weak second peaked around  $+6000 \text{ km s}^{-1}$  is visible in CIV; (3) In the  $Ly\alpha$  profile, a strong core component, which is much less pronounced in the Balmer lines, is present. The variation on the blue side of CIV and  $H\beta$  is similar in both lines. This suggest that the blue sides in the different lines have the same origin, while the prominent red peak seen only in the Balmer lines, is of a different origin. The absence of any correlation of the red peak of  $H\beta$  with the continuum (Veilleux & Zheng, 1991) is in agreement with the notion that this part of the line is not associated with the gas seen in the UV lines and does not respond rapidly to changes in the continuum intensity.

The emission line flux above the continuum was integrated over the corresponding wavelength intervals. The core region in this case is of course strongly contaminated by the important contribution of the narrow line, while the red side of  $Ly\alpha$  is contaminated somewhat by the weak NV  $\lambda 1240$  line. However, the CIV red and blue side are almost free of contamination from any other lines. The total flux of CIV and  $Ly\alpha$  was derived by integration over the full velocity interval from  $-12,000$  to  $+12,000 \text{ km s}^{-1}$ . The line fluxes measured in this way for the emission lines are given in Table 2.

From 1978 to 1993 pointed X-Ray observations of 3C390.3 have been made at 17 epochs with different instruments. The observations from HEAO1-A2, Einstein IPC and MPC are from Malaguti, Bassani & Caroli (1994), while the EXOSAT, and Ginga results are from Inda et al. (1994). The photon spectra were fitted by a single power-law of the form:  $n_{ph}(E) = A E^{-\Gamma} \exp(-\sigma_E N_H)$ , where  $E$ ,  $\sigma_E$  and  $N_H$  are the photon energy, photo-absorption cross sections and the absorption column density, respectively, and  $\Gamma$  is the photon-index. The 4 ROSAT observations taken between 1991 and 1993 were retrieved from the ROSAT database at Max-Planck-Institut für Extraterrestrische Physik and processed independently with EXSAS (Zimmerman et al., 1994). The source counts were extracted from a  $2'$  circle centered on the source centroid. The background is determined from the counts within an annulus of inner radius of  $2'$  and outer radius of  $5'$ . All sources detected with a likelihood greater than 10, defined as the area of  $2'$  radius around the center of light, are excluded from the background, and the exposure time was corrected for the dead time. The gain calibrated source and background counts are corrected individually for vignetting and finally binned in pulse height spectra. The pulse height spectrum is modeled with a single

power-law, folded with Galactic absorption and the detector response function of ROSAT. The absorption cross sections are from Morrison & McCammon (1982). In most cases, a single power-law model fits the spectrum very well (see Table 3). More complicated models, such as a power-law and black-body components, do not improve the quality of the fit and are not justified by the signal-to-noise in the data. The results for all X-ray data are given in Table 3. The results presented here are similar to the high resolution spectral data presented by Eracleous et al. (1996).

The optical spectra used for 3C390.3 were taken at Lick Observatory and calibrated using [OIII] line flux (refer to §2 of Veilleux & Zheng, 1991 for details).

### 3 3. RESULTS

#### 3.1 Variability Pattern

Figure 1 shows the light-curves for the X-rays, the UV continuum at  $1800 \text{ \AA}$  and the CIV line (the lightcurves for  $Ly\alpha$  are very similar in shape to those of CIV, although with smaller amplitude; see Table 4). The UV continuum light curve shows a few large events which typically last one to two years and have amplitudes of up to a factor of 5. They also suggest the presence of smaller and faster events which rise and drop in brightness with a factor of 2 in tens of days. Because of the sparse sampling, most small events can not be resolved and will not be discussed in what follows. The UV continuum reached a maximum state in late 1991 with a subsequent brightness decrease after that. The emission line light curves (see Figure 1) are similar to that of the continuum for the big events, except for the apparent presence of a delay in the peak brightness of some 100 days. After 1988 (JD 2,447,600) the core and red light-curves of CIV and  $Ly\alpha$  show two well-defined events, while in the blue part of the line an additional early peak appears present. This ill-defined first peak in the blue part of the lines is possibly due to the longer response time of blue part (see below §3.3) to a bright state in 1988 which was not observed by IUE. The Ginga observation of November 1988, which is the highest X-Ray flux observed between 1978 and 1993 (see Figure 1), suggests that an additional strong continuum event may have occurred in the latter part of 1988.

During the IUE observations, the UV continuum flux varied by a factor larger than 10 although the actual dynamic range ( $R_{max}$ ) of the continuum variations is difficult to determine due to the fact that the lowest flux, in 1984, is defined by a relatively noisy spectrum (SWP22624). The variability parameters ( $F_{var} = \sigma/\bar{F}$ ) and  $R_{max}$  for line and continuum are given in Table 4. Since  $R_{max}$  is rather uncertain because of the large error associated with the lowest brightness state as well as the sparse temporal coverage in the sampling, we give in Table 4 also  $R_{max} (JD > 7600)$ , which only considers the data taken after 1988. This should give a better evaluation of the variability, since this part of the lightcurve is adequately sampled with respect to the variability time scale. The measurement errors for constant flux (non-variable) source are assumed to be normally distributed and we estimated the error in  $F_{var}$  through a Monte-Carlo calculation for data sets which are consistent with the measurements. It is clear from Table 4 that the UV

continuum shows largest variability parameter, followed by CIV and  $Ly\alpha$ , but note that  $R_{max}$  for CIV is nearly as large as that for the continuum at 1350 Å. The variability parameters for the blue and red-side of the lines are the same within the errors. The core is much less variable than the blue and red side, due to contamination by the narrow line. Correcting for the narrow-line contribution, derived from the regression of the core flux versus continuum relation, both  $F_{var}$  and  $R_{max}$  for the broad line flux in the core, are found to be equal to that of the red and blue sides of the line. Even though the variability parameters at 1350 Å and at 1800 Å are the same within the errors, the short wavelength continuum seems to be more variable than that at 1800 Å.

The mean ultraviolet spectrum is shown in the upper panel of Figure 2, the variance is plotted in the lower panel, and the middle panel shows the normalized variance spectrum (division between the variance spectrum shown in the bottom panel and the average spectrum in the upper panel). The variance spectrum highlights the strong blue asymmetry in the lines also visible in the average spectrum. On the other hand, the flat bottomed depressions in the normalized variance spectrum at the positions of the broad lines indicate that the variation amplitude over the broad lines is essentially the same over the full velocity width of the broad lines. The narrow depressions at the central positions correspond to the, much less variable, narrow lines. The many features between 1820 and 1950 Å (observed wavelength) present in the average spectrum, but absent in the variance spectrum, are most likely associated with the UV FeII blends and contribute at least 10% of the flux in the 1800 Å bandpass.

### 3.2 Time Series Analysis

Cross correlation methods have been used to determine if the variations are correlated and if there is a time lag between continuum and line lightcurves. Two different correlation functions were calculated for the UV light curves of 3C390.3: the interpolated cross correlation function (CCF, Gaskell & Peterson, 1987) and the discrete cross correlation function (DCF, cf. Edelson & Krolik, 1988). We have discarded the data pairs which required interpolated data points with separations larger than 200 days for the calculation of the CCF. The CCF are normalized using only the data points which are used for calculation of CCF at a particular lag (White & Peterson, 1994). The DCF's were calculated as described by White & Peterson (1994).

Firstly, the continuum light-curve at 1800 Å is cross correlated with itself to generate the continuum auto-correlation function (ACF). The continuum light curves are then cross correlated with each line feature light curve to get the corresponding CCF and DCF. Also, the light curves of the different parts of CIV and  $Ly\alpha$  are cross-correlated with each other. To calculate the DCF's, the sampling interval was chosen to be 50 days, which is slightly more than half the average interval of the observations. Figure 3 shows the ACF, as well as the CCF's and DCF's for CIV, with error bars (since the lightcurves for  $Ly\alpha$  are very similar to those of CIV, the correlation functions are too). The ACF of window sampling is overplotted (refer to Gaskell & Peterson, 1987) on the continuum ACF. To the first order, the CCF's and DCF's are in all cases similar, in spite of the

slight differences to be expected for such an unevenly sampled time series (White & Peterson, 1994). Table 5 gives the main characteristics of CCF's. The parameter  $\Delta t_{peak}$  gives the time lag (in days) for  $r_{max}$ , the peak value of CCF. The centroid measures at 0.5  $r_{max}$  give similar results. The errors were calculated with a Monte Carlo (MC) calculation, assuming a Gaussian error distribution and represent the 68% range. The MC calculation was done over a range of  $\pm 500$  days to avoid the overlap of the two individual peaks in the lightcurves at JD7800 and JD8500. This is only significant for the CCF of the core lightcurves, where the amplitude of the emission line lightcurve is significantly reduced by the contribution of the narrow line. A positive value for  $\Delta t_{peak}$  indicates that the variation of the second quantity lags that of the quantity in the first series.

The FWHM of continuum ACF is about 200 days, although larger than the average observation interval (90 days), the sampling is only just below the Nyquist frequency for the long term variability mode. The fact that the FWHM of the ACF for CIV(total) is 400 days, twice the width of continuum ACF, implies that the continuum variation is faster than the light-crossing time of the BLR. This is in good agreement with that inferred from direct inspection of light-curves in Figure 1, especially for the large and reasonably sampled events after 1988. It is clear that emission line and continuum variation are highly correlated, with  $r_{max}$  in the range from 0.7 to 0.9, and the variations of CIV and  $Ly\alpha$  (not shown in Figure 3) lag those of the continuum by about 100 days. Taking the average value of  $\Delta t_{peak}$  for both CIV and  $Ly\alpha$  from Table 5, we find for the red part of the line  $\Delta t_{red} = 57 \pm 18$ ; for the core  $\Delta t_{core} = 80 \pm 41$  and for the blue side  $\Delta t_{blue} = 110 \pm 17$  (average errors, see Table 5). It is thus clear that the red side of both CIV and  $Ly\alpha$  responds significantly earlier to the continuum variation than the blue side. Direct cross correlation of the blue and red sides of the lines, confirms a time delay between the two of  $\Delta t_{R-B} = 46 \pm 17$  days, consistent with the results from the line versus continuum cross correlation. The extra peak in the blue side lightcurve after 1988 (see also §3.1) can now be understood in the context of the differences in the delay between the red and blue sides of the emission lines. The Ginga observation of November 1988 –the highest X-Ray flux observed between 1978 and 1993 (see Figure 1)– suggests the existence of a large continuum event in the latter part of 1988. Since the first UV observation is 130 days after the X-ray peak, this supports the idea that the line response to the 1988 event had already been completed for the red and central parts of the line at the start of the UV observations in 1989, while only the tail end of the response of the blue side of the line was still observed.

### 3.3 Variation of Emission Line Ratio

The CIV/ $Ly\alpha$  line ratio is positively correlated with the continuum flux but shows considerable scatter and is shown in Figure 4(right). This behaviour contrasts with that shown by the other AGN studied in detail where the values of  $R_{max}(CIV/Ly\alpha)$  for NGC 5548 and NGC 3783 are found to be 0.95 and 0.61, respectively as compared to a factor of three in 3C390.3. Also, the CIV/ $Ly\alpha$  ratio tends to decrease slightly with increasing continuum brightness, contrary to the behaviour shown in Figure 4 (right). From Fig-

ure 2 (middle) and Table 4, it is clear that this relation is in part driven by the larger variation in the CIV line as compared to  $Ly\alpha$  (by a factor of two). Regression analysis for the relation between  $Ly\alpha$  and CIV for all components shows that a linear relation between the two lines does not give a statistically significant description of their relation ( $\chi^2_{red} > 1.6$ ).

The correlation with the continuum is better for the red side, for which the Spearman rank correlation coefficient ( $r_s$ ; Press et al., 1986) is 0.67 (corresponding to the null correlation probability  $Pr = 0.3 \times 10^{-5}$ ), than for the blue side ( $r_s=0.58$ ,  $Pr = 10^{-4}$ ). The data after 1988, with a sampling frequency of 80 days for a doubling time of the brightness variations of 250 days can be considered to be sufficiently sampled to describe the variation of the two large events. For these data the correlation disappears for the blue side ( $r_s = 0.207$ ,  $Pr = 0.44$ ) but still persists for the red component ( $r_s = 0.775$ ,  $Pr = 0.4 \times 10^{-3}$ ). This lack of correlation is clearly related to the dissimilar light-curves for the blue side and continuum, and due to the larger delay found for the blue part of the line: the blue sides of both  $Ly\alpha$  and CIV are poorly correlated with  $F_{1800}$  with  $r_s=0.448$  ( $Pr = 0.08$ ) and  $r_s=0.401$  ( $Pr = 0.23$ ) for the data after 1988, but the red side is well correlated with continuum with  $r_s=0.623$  ( $Pr = 0.01$ ) and  $r_s=0.828$  ( $Pr = 10^{-4}$ ), respectively. To overcome the problem due to the delays in line response for the emission lines one could resort to correcting the correlation diagram in Figure 4 (right) for the delay determined above, however the sampling of the lightcurves is not sufficient to apply such correction, as is clearly illustrated by the X-Ray observed event in 1988. An alternative approach to correct the relations for time delay effects, is to use the fact that the CIV line is well correlated with the continuum at similar amplitude, and use the CIV line intensity as a measure of the continuum. Figure 4 (left) shows the CIV/ $Ly\alpha$  ratio for both the red side and the blue side as a function of the blue and red I(CIV), respectively. The relation in Figure 4 (left) is very well defined, in contrast to CIV/ $Ly\alpha$  relation with the continuum, shown in Figure 4 (right), and the CIV/ $Ly\alpha$  ratio for the two sides of the lines merge indistinguishable into each other even though they cover different domains in the diagram (red:  $0 < I(CIV) < 80$  and blue :  $9 < I(CIV) < 120$ , units:  $10^{40} \text{ erg s}^{-1} \text{ cm}^{-2}$ ). This relation shows a tight correlation for the lower intensity levels ( $I(CIV) < 60$  corresponding to  $F_{1800} = 0.6 \cdot 10^{40} \text{ erg s}^{-1} \text{ cm}^{-2} \text{ \AA}^{-1}$ ), while at higher intensities the CIV/ $Ly\alpha$  ratio flattens out and appears to become constant.

### 3.4 Ionizing Continuum Shape

The big blue bump, often seen in the Seyfert galaxies and QSOs, is very weak or absent in 3C390.3. The mean ratio of  $F_\lambda(1350\text{\AA})/F_\lambda(5125\text{\AA})$  for the three nearly simultaneous (within 15 days) observations in optical (19 May 1980, 28 May 1984 and 26 August 1987) and UV (26 May 1980, 5 June 1984 and 12 August 1987) is 4.36 (after correction for the Galactic reddening), corresponding to an optical to UV spectral index ( $F_\nu \propto \nu^{-\alpha}$ )  $\alpha_{optUV} = 0.9$ . The contamination by stellar light in optical is small, because the MgI and FeI absorption features at 5170–5210 are very weak (Veilleux & Zheng, 1991). The mean  $F_\nu(1\text{keV})/F_\nu(1350\text{\AA})$

for 4 UV and X-Ray observations with separation of less than 20 days, is 0.03, corresponding an UV to X-Ray spectral index  $\alpha_{uvx} = 0.89$ .

Although Kruper et al. (1990) claimed the existence of a strong soft X-Ray excess in the Einstein IPC spectrum with a very large absorption, no soft excess is suggested in any of four ROSAT X-Ray observations. The ROSAT spectra can be well modeled by a single power law with a photon spectral slope index in the range between 1.86 to 2.20, very similar to the results of Eracleous et al. (1996). The soft X-ray flux decreased by a factor 2.5 between 1992 and 1993, and the soft X-Ray spectral slope is consistent with a constant value  $\alpha = 0.92 \pm 0.9$ , which is slightly steeper than the spectral index from the Ginga data in the ME band of 0.77 and 0.54 for 1988 and 1991 respectively (Inda et al., 1994). The steeper soft X-ray spectral slope for the observation of 1991 is certainly due to the large fitted  $N_H$  (Table 4). The spectral indices of optical to UV, UV to X-ray, soft X-ray, and ME X-Ray are all very similar for 3C390.3, strongly suggesting that the big blue bump is very weak or absent in this object. The simultaneous observations of 3C390.3 made during the RIASS campaign (de Martino et al., 1992) discussed by Walter et al. (1995) confirm the weakness of the big blue bump in 3C390.3.

It is interesting to note that the spectral energy distribution and the spectra variability character of 3C390.3 from the optical to the X-Rays is quite similar to those found, from extended multi-frequency observations, for the BL Lac object PKS2155-304 (Edelson et al., 1995). The only distinguishing part is the fact that the turnover seen in this BL Lac object at higher energies, is not seen in 3C390.3.

## 4 DISCUSSION

We will here discuss the implications of the results described above in the context of the three questions posed in section 1.

### 4.1 Does the Size BLR scale as $L^{1/2}$ ?

If the BLR in different objects can be characterized by the same physical parameters (ionization parameter  $U$  and particle density  $n_H$ ) and the ionizing continuum shape does not vary much from object to object, the size of BLR scales with continuum luminosity through,

$$r = \left( \frac{N_{ion}}{4\pi c n_H U} \right)^{1/2} \propto L^{1/2}. \quad (1)$$

where  $N_{ion}$  is the number of ionizing photons. Peterson (1993) showed that such a relation may exist for a few Seyfert galaxies with well determined lags. The results of Kaspi (1994), including other Seyfert galaxies and PG quasars, are not in contradiction with this, but the limited temporal sampling in his data, leaves doubtful if this remains valid for the PG quasars, because the high temporal frequencies of the variability are quite undersampled. If the lags found here are considered to represent a good estimate of the BLR size in 3C390.3, it clearly does not fit in the relation defined by these samples. The mean UV luminosity at  $1340\text{\AA}$  for 3C390.3 is  $L_\lambda = 2 \cdot 10^{40} \text{ erg s}^{-1} \text{ \AA}^{-1}$  ( $h_0 = 1.0$ , as adopted in Peterson, 1993), which is the same as for NGC5548, but CIV variations for NGC 5548 show a lag of

about 8 days versus the 63 days for the total line integral for 3C390.3 (see Table 5), suggesting a BLR size some 8 times larger in 3C390.3. It should be kept in mind that lags of the order of those found in the campaign on NGC 5548 (4-30 days) can not be found in the data for 3C390.3 discussed here, since the average sampling interval of  $89 \pm 57$  days (ignoring the 4 intervals in excess of one year) will not permit the determination of such small delays. This does however not invalidate the larger delays found here, since the sampling for the two large events after 1988 appears to be adequate for the characteristic variability time scale of some 250 days.

The breakdown of  $r \propto L^{1/2}$  implies that one or more of the assumptions, on which the Size–Luminosity relation is based, are invalid for 3C390.3: (1) The product  $n_H U$  in 3C390.3 is a factor of 60 less than in other AGNs monitored previously; (2) The number of ionizing photons  $N_{ion}$  striking the BLR in 3C390.3 is 50 times more than simple scaling UV continuum would predict.

More ionizing photons could be a result of the hard ionizing continuum. If the continuum incident on the BLR clouds is the same as what we observe –without a big blue bump–, the ionizing continuum is much harder than that in other Seyfert galaxies as discussed in §3. Even if this is the case, the total number of ionizing continuum photons in 3C390.3 is estimated to be a only factor  $\sim 4$  larger than that in NGC5548 (taking  $\alpha_{uvx} = 0.8$ , and 1.5 for 3C390.3 and NGC5548 respectively), much less than what is needed to account for the large observed delay. With equal covering factors for these two objects, this estimate of the ionizing photon flux  $N_{ion}$  is consistent with the observed values of  $EW(Ly\alpha)$  and  $EW(CIV)$ , which are a factor of  $\sim 3$ –4 larger in 3C390.3 than in NGC5548. Alternatively, the continuum in other directions could be much stronger than observed, due to the anisotropic emission. However, this would cause an increase in the equivalent widths of the emission lines as well. The  $EW(Ly\alpha)$  and  $EW(CIV)$  limit the degree of anisotropy for the ionizing continuum toward BLR. The continuum in the direction of BLR can not be a factor of 10 larger for any reasonable value for the covering factor. Therefore,  $n_e U$  must be an order of magnitude less in 3C390.3 than in NGC 5548.

If the continuum emission is isotropic, the total luminosity of 3C390.3 integrated from optical to X–Ray (assuming it extends to 500 keV) will be in the range 0.13 to 1.8  $10^{45}$  erg  $s^{-1}$  (corresponding to the observed variability), which is well within the range of the Eddington luminosity for a  $10^9$  solar mass black hole ( $0.001$ – $0.01 L_{Edd}$ ). The luminosity in the UV and optical range is only a fraction of this, and therefore fully compatible with the accretion rates which can be sustained in an ion-supported torus (Begelman, 1986). The infrared spectrum peaking at  $25 \mu m$  in this object would than represent the synchrotron self absorption of an ion torus, as already suggested by Chen & Halpern (1988). The absence of a thermal big blue bump implies that a possible disk is not cooling down via thermal radiation, but rather via inverse Compton scattering of low energy photons, consistent with ion-torus model (Rees et al., 1982).

## 4.2 The CIV/Ly $\alpha$ Ratio

The results shown in Figure 4 for the CIV/Ly $\alpha$  variations can be easily understood in the context of the continuum variation as described above in absence of a big blue bump component in the continuum incident on the BLR clouds. In NGC5548, F9 and 3C120, both the ratio CIV/Ly $\alpha$  and the EW(CIV) decreases as the continuum flux increases (Pogge & Peterson, 1992; Clavel, Wamsteker & Glass, 1989; Gondhalekar, 1992). This behavior is exactly the opposite of the usual prediction and has been interpreted as an indication that the big blue bump does not continue to rise with photon energy, but rolls over at energies higher than 10 eV, and a second hard component is less variable (Binnete et al., 1989; Clavel & Santos-Lleó, 1990; also Maoz, Peterson & Netzer, 1994). However, Shields et al. (1995) showed that such decrease in the CIV/Ly $\alpha$  ratio could also result from a partially optically thin BLR (their “Wamsteker–Colina” effect). The results found here suggest that we are seeing the effect of the hard continuum on a mixed medium of thin and thick clouds, as suggested by Shields et al. (1995). The very steep increase at low luminosity would then correspond to the an increase in the ionizing fraction of CIV in the thin cloud, while this will not be accompanied by a major increase in the Ly $\alpha$  emission. However, when the ionization parameter becomes higher, the thick clouds will start to dominate the emission, with the consequent flattening of the CIV/Ly $\alpha$  ratio, since the intensity increase in the thick BLR clouds is similar for both Ly $\alpha$  and CIV. This could e.g. be associated with deeper penetration of the Ly $\alpha$  ionization front as compared to the CIV ionization front at low brightness levels. The consequence of this scenario for 3C390.3 is that, in comparison with most of the previously studied radio–quiet AGN’s, the optically thin material in the BLR must be of much greater importance here. This is the first time that a real difference in the nature of the BLR clouds in a radio–loud and radio–quiet AGN’s is indicated.

## 4.3 Kinematics of BLR

With a central source of ionizing radiation, the obvious consequence of the fact that the variation in red side of CIV precedes that in the blue side is, that the gas moving away from us is located between the observer and the source of ionizing radiation, while the blue side of the line is originating on the far side of the central source, i.e. gas infall towards the center. A simple spherical symmetrical inflow model predicts,  $\tau_{blue} = 3\tau_{red}$ . This might still be in agreement with the observations with  $\tau_{red} = 57 \pm 18$  days and  $\tau_{blue} = 110 \pm 17$  days, but the results suggest more something like  $\tau_{blue} \simeq 2 \times \tau_{red}$ . Since many previous observational results do suggest the presence of anisotropy in either the radiation field and/or the material distribution, we will for the following discussion assume a disk configuration of the material in the BLR. In this case *some form of rotational symmetry* is indicated and the difference in the delays then places the broad-line emitting material on opposite sides of such disk. The difference in time delay between the blue and red wings of the lines allows us to determine their projection on the sky, which we find to be  $18^{+10}_{-23}$  degrees (i.e. the angle between the l.o.s. and the direction connecting the blue and red wing emitting material, not necessarily equal

to the inclination of a possible disk, is  $72_{-10}^{+13}$  degrees). The actual size of the measured delay then places the BLR material at a distance of  $83 \pm 25$  lightdays from the central source. Assuming that these regions are in rotation around the center of mass associated with the continuum source, the difference in velocity between the blue and the red sides is the combined effect of rotational and radial motion. Taking the peak in the variance spectrum of the CIV line to represent the mean line-of-sight velocity of  $3000 \text{ km s}^{-1}$  for both the redshifted and blue-shifted material in the BLR, we find a purely rotational component of the velocity field of the BLR of  $v_{\text{circ}} = 2850_{-700}^{+1000} \text{ km s}^{-1}$ , combined with an infall velocity of  $v_{\text{infall}} = 950_{-500}^{+1000} \text{ km s}^{-1}$  (errors represent the uncertainty in the projection angle above). Such a systematic velocity field and infall in the BLR also supplies a mechanism to allow the natural removal of angular momentum from the BLR as a consequence of the preferential escape from the system of material, with the largest random velocities, in the direction of the systematic rotation. The existence of ordered rotational motion in bound orbits at a distance of  $R_{\text{BLR}} = 2.2 \cdot 10^{17} \text{ cm}$  from the central source permits, under the assumption that we are seeing the disk edge-on, the determination of a *lower limit* to the central mass of  $M_{\text{CM}} > 1.3 \cdot 10^8 M_{\odot}$ . In the presence of ordered bound rotational motion around a central mass the FWHM of the broad lines corresponds to the escape velocity from the central mass, which places an *upper limit* to the central mass, within the radius of the BLR of  $R_{\text{BLR}} = 0.07 \text{ pc}$ , of  $M_{\text{CM}} < 4.0 \cdot 10^8 M_{\odot}$ .

In conclusion we find here that the central mass is confined between  $1.3 \cdot 10^8 M_{\odot} < M_{\text{CM}} < 4.0 \cdot 10^8 M_{\odot}$ , which places the BLR in 3C390.3 at a distance of  $500 \pm 150 R_{\text{Schwarzschild}} < R_{\text{BLR}} < 1,500 \pm 500 R_{\text{Schwarzschild}}$ , with an orbital period of some 150 years, which is only twice the infall time towards the center at the infall velocity of  $950 \text{ km s}^{-1}$ . These limits on the BLR size can be compared with those derived by Eracleous and Halpern (1994) on the basis of detailed accretion disk model fits to the outer wings of  $H\alpha$ . They found  $380 R_{\text{Schwarzschild}} < R_{\text{BLR}} < 1,300 R_{\text{Schwarzschild}}$ , with a disk inclination (the angle between the line-of-sight and the normal to the disk) of  $26_{-2}^{+4}$  degrees. Using the superluminal motions in the jet of 3C390.3, Eracleous et al. (1996) determined the angle of ejection of the radio blobs and the line-of-sight, which was found to be between 19 and 33 degrees. Our implicit assumptions for the results from the UV data, only required rotational symmetry. However, since generally speaking, the broad emission lines should all come from the BLR (even though this may be stratified), the only way in which these results are consistent with those from the UV lines discussed here, is if the angular projection angle for the blue and red parts of the UV lines of  $18_{-23}^{+10}$  degrees is considered to be an independent measure of the inclination of the disk required for the  $H\alpha$  line. Combing these angular results, we see that in 3C390.3 we have for the first time strong *observational* evidence that the BLR emission is associated with an accretion disk and the superluminal motions take place orthogonal to the plane of this disk ( $98 \pm 12$  degrees). In such configuration (see Figure 6), if the full line width of Fe  $K\alpha$  emission would be due to Doppler broadening from the motion in the disk (Eracleous et al., 1996), the Fe  $K\alpha$  would be emitted in a region at a distance  $< 400 R_{\text{Schwarzschild}}$ ,

corresponding to the inner edge of the BLR as found from the UV lines. One caveat for this conclusion could be the strong evidence for optically thin gas found here (see Figure 4), which may have an effect on the modeling of the Fe  $K\alpha$  emission, which has not been taken into consideration by Eracleous et al. (1996).

The variations in the relative contributions to the total line profile of the differently behaved velocity components in 3C390.3 could easily explain the large blue shifts in CIV and  $Ly\alpha$ , often seen in luminous quasars, relative to low ionization lines such as OI and MgII (Gaskell, 1982; Espey et al., 1989; Corbin, 1990). Ferland et al. (1992) have shown that the line emission from thick clouds is anisotropic with preferred emission from the clouds in the direction of the ionizing source (see also Ferland & Netzer, 1979). Our results then suggest that the material farthest from us would dominate the line profiles, since they are illuminated by the central source from a direction close to our viewing angle, giving rise to the strong line strength asymmetries seen in Figure 2 for 3C390.3.

## 5 SUMMARY AND CONCLUSIONS

We have described the results of an analysis IUE, optical and X-Ray observations of 3C390.3. The main results are:

1. The variations of the total intensity of the CIV and  $Ly\alpha$  lines lag behind those of UV continuum by some 66 days, which is a factor of 8 larger than one would expect by simply scaling  $r \propto L^{1/2}$  from the data of other Seyfert galaxies.
2. The red side of both the  $Ly\alpha$  and the CIV lines responds to continuum variations faster than the blue side by about  $46 \pm 17$  days. This results under rotational symmetry to a distance of the BLR to the central source of  $R_{\text{BLR}} = 83 \pm 25$  lightdays. Assuming rotational motion, and since the differential delay indicates infall, this suggests a large infalling component of  $950_{-500}^{+1000} \text{ km s}^{-1}$  in the BLR velocity field with a pure rotational component of  $2850_{-700}^{+1000} \text{ km s}^{-1}$ . From this we conclude the central mass to be confined to  $1.3 \cdot 10^8 M_{\odot} < M_{\text{CM}} < 4.0 \cdot 10^8 M_{\odot}$ .
3. From an analysis of the optical, UV and X-Ray spectrum, no big blue bump or soft X-Ray excess is found in 3C390.3. The continuum spectrum from the optical to the X-rays can be described by a single power law with index  $\alpha \simeq -0.90$ .
4. The CIV/ $Ly\alpha$  ratio increases as the continuum brightens and flattens off at high continuum levels, consistent with the expected behavior under photoionization of a mixed cloud composition of optically thin and thick clouds, with a constant continuum shape. This is also consistent with the absence of a big blue bump in the spectral energy distribution of 3C390.3 and indicates for the first time a difference in the BLR of a radio-loud AGN as compared to the radio-quiet Seyfert I galaxies.
5. The blue part in the CIV,  $Ly\alpha$  and Balmer lines originates in the same emitting material, but the red peak in  $H\beta$  does not respond to the continuum variations and therefore is different, most likely at considerably larger distance.
6. The physical dissociation and the different delays for

the blue and red sides of the broad emission lines under rotational symmetry, suggests that we see the blue part of the BLR clouds face-on with the red part more in a back-illuminated geometry. This supplies a logical explanation for the blue shifts seen in the high luminosity QSO's with respect to the narrow lines, since the blue part of the originates in clouds seen from the directly illuminated side.

7. Comparing our results with recent ASCA observations by Eracleous et al. (1996) our results are fully consistent with theirs if the UV lines are emitted in an accretion disk, where the Fe  $K\alpha$  is emitted at the inner edge of the disk with a disk inclination between 18 and 30 degrees, and the superluminal radio blobs moving orthogonal to the plane of the disk associated with the BLR.

## ACKNOWLEDGMENTS

We are indebted to D. Osterbrock, J. Miller and S. Veilleux for providing the optical spectra of 3C390.3. TW would like to thank Jean Clavel for many stimulating discussions and help in the IUE data processing. We thank the anonymous referee for his comments, which significantly contributed to the presentation of the data. TW wishes to acknowledge the support of the ESA IUE Observatory at VILSPA, and financial support from the Pedan Project of Chinese Scientific Committee and Chinese National Natural Science Foundation.

## REFERENCES

- Alef, W., Goetz, M.M.A., Preuss, E., & Kellermann, K.I. 1988, *S&A*, 192, 53
- Begelman, M.C. 1986, in *Astrophysics of Active Galaxies and Quasi-Stellar Objects*, ed. Miller, J.S.
- Binnette, L., Prieto, A., Szuszkiewicz E. & Zheng, W. 1989, *ApJ*, 343, 135
- Chen, K. & Halpern, J.P. 1989, *ApJ*, 344, 115
- Clavel, J., & Santos-Lleó, M. 1988, *A&A*, 230, 3
- Clavel, J. & Wamsteker, W. 1987, *ApJ*, 320, L9
- Clavel, J., Wamsteker, W., & Glass, I.S. 1989, *ApJ*, 337, 236
- Clavel, J., et al. 1991, *ApJ*, 366, 64
- Clavel, J., et al. 1990, *MNRAS*, 246, 668
- Corbin, M.R. 1990, *ApJ*, 357, 346
- Courvosier, Th.J.-L., & Paltini, S., 1992, *IUE-ULDA Access Guide No.4*,  
Ed. W.Wamsteker, ESA SP 1153
- Crenshaw, D.M., et al. 1994, *ApJ*, submitted
- de Martino, D., et al., 1991, *ESA IUE Newsletter*, No.38,10
- Edelson, R.A. & Krolik, J.H. 1988, *ApJ*, 333, 646
- Eracleous, M., Halpern, J.P., Livio, M., 1996, *ApJ*, 459, 89
- Eracleous, M. & Halpern, J.P., 1994, *ApJS*, 90, 1
- Espey, B.R., Carswell, R.F., Bailey, J.A., Smith, M.G., & Ward, M.J. 1989  
*ApJ*, 342, 666
- Ferland, G., & Netzer, H. 1979, *ApJ*, 229, 274
- Ferland, G., Peterson, B.M., Horne, K., Welsh, W.F. & Nahar, S.N. 1992, *ApJ*, 387, 95
- Gaskell, C.M. 1982, *ApJ*, 263, 483
- Gaskell, C.M. & Peterson, B.M., 1987, *ApJS*, 65, 1
- Gondhalekar, P.M. 1992, *MNRAS*, 255, 663
- Inda, M., Makishima, K., Kohmura, Y., Tashiro, M., Ohashi, Bar, P., et al. 1994,  
*ApJ*, 420, 143
- Kallman, T.R., & Krolik, J.H. 1986, *ApJ*, 308, 805
- Kaspi, S. 1994, M.Sc. thesis, Tel-Aviv University
- Koratkar, A.P., & Gaskell, C.M. 1991, *ApJS*, 75, 719
- Korista, K.T., et al. 1995, *ApJS*, 97, 285
- Kruper, J.S., Urry, C.M., & Canizares, C.R. 1990, *ApJS*, 74, 347
- Lloyd, C. 1984, *MNRAS*, 209, 697
- Malaguti, G., Bassani, L., & Caroli, E. 1994, *ApJS*, 94, 517
- Miley, G., et al. 1984, *ApJ*, 278, L79
- Morrison, McCammon, 1983, *ApJ*, 270, 119
- Osterbrock, D., Koski, A.T., & Phillips, M.M. 1976, *ApJ*, 206, 898
- Perez, E., Penston, M.V., Tadhunter, C., Mediavilla, E., & Moles, M.  
1988, *MNRAS*, 230, 253
- Peterson, B.M. 1993, *PASP*, 105, 247
- Peterson, B.M., et al. 1991, *ApJ*, 368, 119
- Peterson, B.M., et al. 1992, *ApJ*, 392, 470
- Recondo, M.C., et al., 1997, *A&AS*, in press
- Reichert, G.A., et al. 1994, *ApJ*, 425, 582
- Rodriguez-Pascual, P.M., 1997, *ApJ*, in press
- Seaton, M.J., 1979, *MNRAS*, 187, 73P
- Shields, J.C., Ferland, G.J., & Peterson, B.M. 1995, *ApJ*, 441, 507
- Stirpe, C.M., et al. 1994, *ApJ*, 425, 609
- Veilleux, S., & Zheng, W. 1991, *ApJ*, 377, 89
- Walter, R., et al., 1994, *A. & A.*, 285, 119
- Wamsteker, W. & Colina, L. 1986, *ApJ*, 311, 617
- Wamsteker, W. & Clavel, J., 1989, *IAU Circ.* 4763
- Wamsteker, W., et al., 1990, *ApJ*, 354, 446
- Wanders, I., et al., 1995, *ApJ. Lett.*, 453, L87
- White, R.J., & Peterson, B.M. 1994, *PASP*, 106, 879
- Wilkes, B.J. 1986, *MNRAS*, 218, 331
- Zheng, W., Veilleux, S., & Grandi, S.A. 1991, *ApJ*, 381, 418
- Zheng, W., 1996, *Astron. J.*, in press.
- Zimmermann, H.U., et al. 1994, *EXSAS User's Guide*, MPE Report 257



**Table 1.** IUE Observation Log and Continuum Flux

No.	Julian date	date	$F_{\lambda}(1340\text{\AA})$ $10^{-14}\text{erg s}^{-1}\text{cm}^{-2}\text{\AA}^{-1}$	$F_{\lambda}(1820\text{\AA})$
	-2,440,000			
1	3,833	21Nov78	0.65±0.28	0.43±0.15
2	3,840	28Nov78	0.89±0.66	-----
3	3,920	16Feb79	0.49±0.37	0.32±0.13
4	3,965	02Apr79	0.40±0.47	0.43±0.26
5	3,969	06Apr79	0.59±0.37	0.37±0.22
6	4,385	26May80	0.35±0.33	0.34±0.19
7	4,577	04Dec80	0.39±0.33	0.37±0.17
8	4,600	27Dec80	0.62±0.24	0.45±0.10
9	4,634	30Jan81	0.40±0.35	0.37±0.22
10	5,176	26Jul82	0.31±0.40	0.28±0.17
11	5,280	07Nov82	0.15±0.25	0.09±0.42
12	5,421	28Mar83	0.28±0.26	0.24±0.12
13	5,600	23Sep83	0.51±0.28	0.38±0.15
14	5,789	30Mar84	0.15±0.42	0.19±0.32
15	5,856	05Jun84	0.32±0.24	0.18±0.09
16	5,939	27Aug84	0.35±0.32	0.19±0.13
17	6,150	26Mar85	0.92±0.23	0.55±0.11
18	6,672	30Aug86	0.52±0.39	0.48±0.13
19	6,823	28Jan87	0.43±0.37	0.34±0.14
20	6,951	05Jun87	0.51±0.29	0.34±0.13
21	7,019	12Aug87	0.68±0.33	0.53±0.14
22	7,160	31Dec87	0.54±0.34	0.56±0.19
23	7,207	16Feb88	0.32±0.16	0.31±0.18
24	7,607	22Mar89	0.73±0.28	0.41±0.14
25	7,655	09May89	0.56±0.25	0.36±0.10
26	7,752	14Aug89	0.71±0.41	0.80±0.15
27	7,843	13Nov89	0.81±0.32	0.99±0.19
28	7,920	29Jan90	0.83±0.28	0.55±0.12
29	7,939	17Feb90	0.78±0.26	0.46±0.12
30	7,998	17Apr90	0.84±0.51	0.61±0.20
31	8,083	11Jul90	0.62±0.17	0.39±0.07
32	8,133	30Aug90	0.49±0.20	0.40±0.13
33	8,135	01Sep90	0.51±0.18	0.36±0.09
34	8,253	28Dec90	1.26±0.31	0.86±0.24
35	8,369	23Apr91	0.99±0.23	0.73±0.12
36	8,499	31Aug91	2.37±0.31	1.35±0.12
37	8,634	13Jan92	1.43±0.26	0.89±0.15
38	8,661	09Feb92	0.96±0.23	0.67±0.09
39	8,762	20May92	0.62±0.24	0.50±0.14

**Table 2.** UV Line Fluxes

No.	Ly $\alpha$		CIV					
	blue	centre	red	total				
	$10^{-14} \text{ erg cm}^{-2} \text{ s}^{-1}$							
1	80 $\pm$ 5	172 $\pm$ 9	60 $\pm$ 5	348 $\pm$ 21	38 $\pm$ 4	65 $\pm$ 4	13 $\pm$ 4	131 $\pm$ 17
2	47 $\pm$ 5	147 $\pm$ 8	80 $\pm$ 6	299 $\pm$ 53	57 $\pm$ 15	73 $\pm$ 10	46 $\pm$ 15	207 $\pm$ 66
3	62 $\pm$ 4	155 $\pm$ 8	67 $\pm$ 5	306 $\pm$ 21	38 $\pm$ 4	67 $\pm$ 4	34 $\pm$ 4	157 $\pm$ 20
4	67 $\pm$ 7	173 $\pm$ 9	66 $\pm$ 7	336 $\pm$ 27	45 $\pm$ 6	60 $\pm$ 5	36 $\pm$ 6	190 $\pm$ 28
5	61 $\pm$ 9	140 $\pm$ 9	54 $\pm$ 9	272 $\pm$ 22	45 $\pm$ 5	59 $\pm$ 4	17 $\pm$ 5	140 $\pm$ 23
6	57 $\pm$ 5	145 $\pm$ 8	48 $\pm$ 4	274 $\pm$ 20	13 $\pm$ 4	42 $\pm$ 3	8 $\pm$ 4	71 $\pm$ 19
7	46 $\pm$ 5	132 $\pm$ 7	53 $\pm$ 5	258 $\pm$ 19	26 $\pm$ 4	51 $\pm$ 4	19 $\pm$ 4	111 $\pm$ 19
8	44 $\pm$ 4	123 $\pm$ 6	66 $\pm$ 4	251 $\pm$ 16	22 $\pm$ 3	47 $\pm$ 3	16 $\pm$ 3	103 $\pm$ 13
9	51 $\pm$ 4	120 $\pm$ 6	46 $\pm$ 4	229 $\pm$ 20	34 $\pm$ 5	57 $\pm$ 4	29 $\pm$ 5	144 $\pm$ 22
10	45 $\pm$ 5	142 $\pm$ 8	49 $\pm$ 5	254 $\pm$ 21	15 $\pm$ 5	46 $\pm$ 4	10 $\pm$ 5	74 $\pm$ 21
11	35 $\pm$ 3	113 $\pm$ 6	34 $\pm$ 3	192 $\pm$ 21	14 $\pm$ 5	39 $\pm$ 4	11 $\pm$ 5	75 $\pm$ 25
12	45 $\pm$ 3	111 $\pm$ 6	33 $\pm$ 3	201 $\pm$ 15	13 $\pm$ 3	35 $\pm$ 3	13 $\pm$ 3	69 $\pm$ 14
13	49 $\pm$ 4	121 $\pm$ 6	44 $\pm$ 4	226 $\pm$ 17	29 $\pm$ 4	40 $\pm$ 3	20 $\pm$ 4	103 $\pm$ 16
14	40 $\pm$ 6	110 $\pm$ 6	33 $\pm$ 5	193 $\pm$ 23	17 $\pm$ 6	39 $\pm$ 4	9 $\pm$ 6	83 $\pm$ 27
15	34 $\pm$ 3	90 $\pm$ 5	25 $\pm$ 3	151 $\pm$ 12	11 $\pm$ 3	30 $\pm$ 2	11 $\pm$ 3	61 $\pm$ 12
16	16 $\pm$ 3	70 $\pm$ 4	24 $\pm$ 3	113 $\pm$ 14	9 $\pm$ 4	20 $\pm$ 3	2 $\pm$ 4	32 $\pm$ 16
17	53 $\pm$ 5	109 $\pm$ 6	46 $\pm$ 4	239 $\pm$ 15	37 $\pm$ 3	42 $\pm$ 3	32 $\pm$ 3	144 $\pm$ 14
18	44 $\pm$ 4	105 $\pm$ 6	44 $\pm$ 4	212 $\pm$ 18	22 $\pm$ 4	29 $\pm$ 3	18 $\pm$ 4	90 $\pm$ 20
19	67 $\pm$ 5	121 $\pm$ 7	46 $\pm$ 5	248 $\pm$ 19	40 $\pm$ 5	41 $\pm$ 3	29 $\pm$ 4	139 $\pm$ 20
20	73 $\pm$ 5	125 $\pm$ 7	44 $\pm$ 3	257 $\pm$ 18	25 $\pm$ 4	39 $\pm$ 3	23 $\pm$ 4	104 $\pm$ 16
21	59 $\pm$ 4	126 $\pm$ 7	43 $\pm$ 4	237 $\pm$ 18	36 $\pm$ 4	47 $\pm$ 3	29 $\pm$ 4	129 $\pm$ 18
22	55 $\pm$ 5	110 $\pm$ 6	43 $\pm$ 4	207 $\pm$ 18	17 $\pm$ 4	45 $\pm$ 4	16 $\pm$ 4	80 $\pm$ 19
23	69 $\pm$ 4	108 $\pm$ 6	42 $\pm$ 3	235 $\pm$ 15	31 $\pm$ 3	40 $\pm$ 3	18 $\pm$ 3	93 $\pm$ 13
24	102 $\pm$ 6	149 $\pm$ 8	66 $\pm$ 5	334 $\pm$ 21	75 $\pm$ 5	70 $\pm$ 4	40 $\pm$ 4	209 $\pm$ 19
25	99 $\pm$ 5	146 $\pm$ 7	61 $\pm$ 4	326 $\pm$ 19	68 $\pm$ 4	62 $\pm$ 4	33 $\pm$ 3	179 $\pm$ 15
26	96 $\pm$ 7	154 $\pm$ 8	80 $\pm$ 6	367 $\pm$ 24	64 $\pm$ 5	73 $\pm$ 5	49 $\pm$ 5	215 $\pm$ 23
27	112 $\pm$ 6	180 $\pm$ 9	81 $\pm$ 5	411 $\pm$ 25	81 $\pm$ 6	81 $\pm$ 5	50 $\pm$ 5	243 $\pm$ 22
28	86 $\pm$ 5	158 $\pm$ 8	92 $\pm$ 5	368 $\pm$ 22	67 $\pm$ 5	75 $\pm$ 4	48 $\pm$ 4	217 $\pm$ 18
29	102 $\pm$ 6	147 $\pm$ 8	69 $\pm$ 5	335 $\pm$ 20	80 $\pm$ 5	70 $\pm$ 4	35 $\pm$ 4	206 $\pm$ 17
30	82 $\pm$ 5	117 $\pm$ 6	62 $\pm$ 5	285 $\pm$ 25	62 $\pm$ 6	62 $\pm$ 5	36 $\pm$ 6	181 $\pm$ 27
31	78 $\pm$ 4	108 $\pm$ 5	53 $\pm$ 3	257 $\pm$ 15	48 $\pm$ 3	51 $\pm$ 3	28 $\pm$ 2	143 $\pm$ 11
32	64 $\pm$ 4	123 $\pm$ 6	47 $\pm$ 3	250 $\pm$ 16	35 $\pm$ 3	42 $\pm$ 3	25 $\pm$ 3	117 $\pm$ 13
33	65 $\pm$ 4	124 $\pm$ 6	53 $\pm$ 4	257 $\pm$ 15	36 $\pm$ 3	41 $\pm$ 3	23 $\pm$ 2	115 $\pm$ 12
34	76 $\pm$ 7	123 $\pm$ 7	48 $\pm$ 6	261 $\pm$ 20	43 $\pm$ 5	61 $\pm$ 4	40 $\pm$ 5	183 $\pm$ 22
35	96 $\pm$ 6	141 $\pm$ 7	65 $\pm$ 4	330 $\pm$ 19	56 $\pm$ 4	62 $\pm$ 4	42 $\pm$ 3	191 $\pm$ 16
36	104 $\pm$ 7	157 $\pm$ 8	94 $\pm$ 7	389 $\pm$ 23	79 $\pm$ 5	84 $\pm$ 5	69 $\pm$ 5	268 $\pm$ 20
37	158 $\pm$ 8	195 $\pm$ 10	101 $\pm$ 6	489 $\pm$ 27	116 $\pm$ 7	104 $\pm$ 6	79 $\pm$ 5	342 $\pm$ 23
38	150 $\pm$ 8	182 $\pm$ 9	96 $\pm$ 6	464 $\pm$ 25	107 $\pm$ 6	92 $\pm$ 5	66 $\pm$ 4	307 $\pm$ 19
39	122 $\pm$ 7	162 $\pm$ 8	76 $\pm$ 5	382 $\pm$ 22	96 $\pm$ 6	80 $\pm$ 4	49 $\pm$ 4	244 $\pm$ 19

**Table 3.** X-Ray Data and nearest UV Continuum Flux

Date	Instrument	A(0.01) <sup>a</sup>	$\Gamma$	$\Delta t_{uvx}$	$N_H^b$	$\chi^2/\text{d.o.f.}$
781121	HEAO2/MPC	0.37	1.3±0.24	0		
781224	HEAO1/A2	0.74	1.65±0.30	-34		
781224	HEAO1/A4	0.78	1.40±0.37	-34		
800101	HEAO2/IPC	0.60 <sup>+0.77</sup> <sub>0.26</sub>	2.75 <sup>+0.53</sup> <sub>-0.44</sub>	60.3±1.9		
800408	HEAO2/MPC	0.18	1.40 <sup>+0.51</sup> <sub>-0.37</sub>	56		
830904	EXOSAT/ME	0.69±0.23	1.68 <sup>+0.20</sup> <sub>-0.08</sub>	19		36/33
840602	EXOSAT/ME	0.29 <sup>+0.33</sup> <sub>-0.14</sub>	2.5±0.7	2		27/18
850202	EXOSAT/ME	0.51±0.15	1.75±0.2	55		37/35
851107	EXOSAT/ME	0.57±0.12	1.70±0.2	–		26/32
860316	EXOSAT/ME	0.44±0.01	1.60±0.10	168		27/32
860317	EXOSAT/ME	0.43±0.05	1.57±0.08	167		21/36
881111	Ginga	1.29±0.03	1.77±0.01	120		40.1/37
910214	Ginga	0.51±0.02	1.54±0.02	47		45.0/35
910330	ROSAT	0.58±0.01	1.86±0.07	24	5.93±0.35	27.1/17
920411	ROSAT	1.00±0.06	1.88±0.08	38	5.84±0.85	13.0/15
930411	ROSAT	0.39±0.06	1.90±0.09	–	6.74±0.70	18.4/14
930412	ROSAT	0.41±0.03	2.21±0.11	–	8.14±1.35	7.75/13

a. A(0.01) = A/(0.01 photon cm<sup>-2</sup>s<sup>-1</sup>keV<sup>-1</sup>) at 1 keV  
 b. in unit of 10<sup>20</sup> cm<sup>-2</sup>

**Table 4.** Variability Parameters

Feature	Mean flux	$F_{var}$	$R_{max}$	$R_{max}(> JD7600)$
F $\lambda$ (1350Å)	0.91	0.42±0.09	15.8	7.4
F $\lambda$ (1800Å)	0.38	0.38±0.05	7.1	4.4
<i>Ly</i> $\alpha$ total	344	0.20±0.02	4.3	2.4
<i>Ly</i> $\alpha$ blue	100	0.26±0.02	9.9	2.9
<i>Ly</i> $\alpha$ core	148	0.16±0.01	2.8	1.9
<i>Ly</i> $\alpha$ red	72	0.24±0.02	4.2	2.9
CIV total	210	0.28±0.02	11.7	4.3
CIV blue	70	0.33±0.02	12.9	6.8
CIV core	69	0.24±0.02	5.2	2.7
CIV red	45	0.35±0.03	::	4.9

**Table 5.** Main Characteristics of Cross Correlations

First Series	Second Series	$\Delta t_{peak}$ (Days) (1)	$r_{max}$
F $\lambda$ (1800Å)	<i>Ly</i> $\alpha$ blue	108 <sup>+15</sup> <sub>-21</sub>	0.84
F $\lambda$ (1800Å)	<i>Ly</i> $\alpha$ core	88 <sup>+49</sup> <sub>-37</sub>	0.78
F $\lambda$ (1800Å)	<i>Ly</i> $\alpha$ red	66 <sup>+22</sup> <sub>-21</sub>	0.84
F $\lambda$ (1800Å)	<i>Ly</i> $\alpha$ total	69 <sup>+50</sup> <sub>-19</sub>	0.81
F $\lambda$ (1800Å)	CIV blue	111 <sup>+18</sup> <sub>-13</sub>	0.84
F $\lambda$ (1800Å)	CIV core	71 <sup>+49</sup> <sub>-31</sub>	0.82
F $\lambda$ (1800Å)	CIV red	49 <sup>+13</sup> <sub>-17</sub>	0.87
F $\lambda$ (1800Å)	CIV total	63 <sup>+57</sup> <sub>-20</sub>	0.84
<i>Ly</i> $\alpha$ red	<i>Ly</i> $\alpha$ blue	48 <sup>+20</sup> <sub>-19</sub>	0.94
CIV red	CIV blue	45 <sup>+17</sup> <sub>-18</sub>	0.85

(1) The formal errors (Gaskell and Peterson, 1987) in the correlation functions (CCF and DCF) are  $\pm 15$  days.

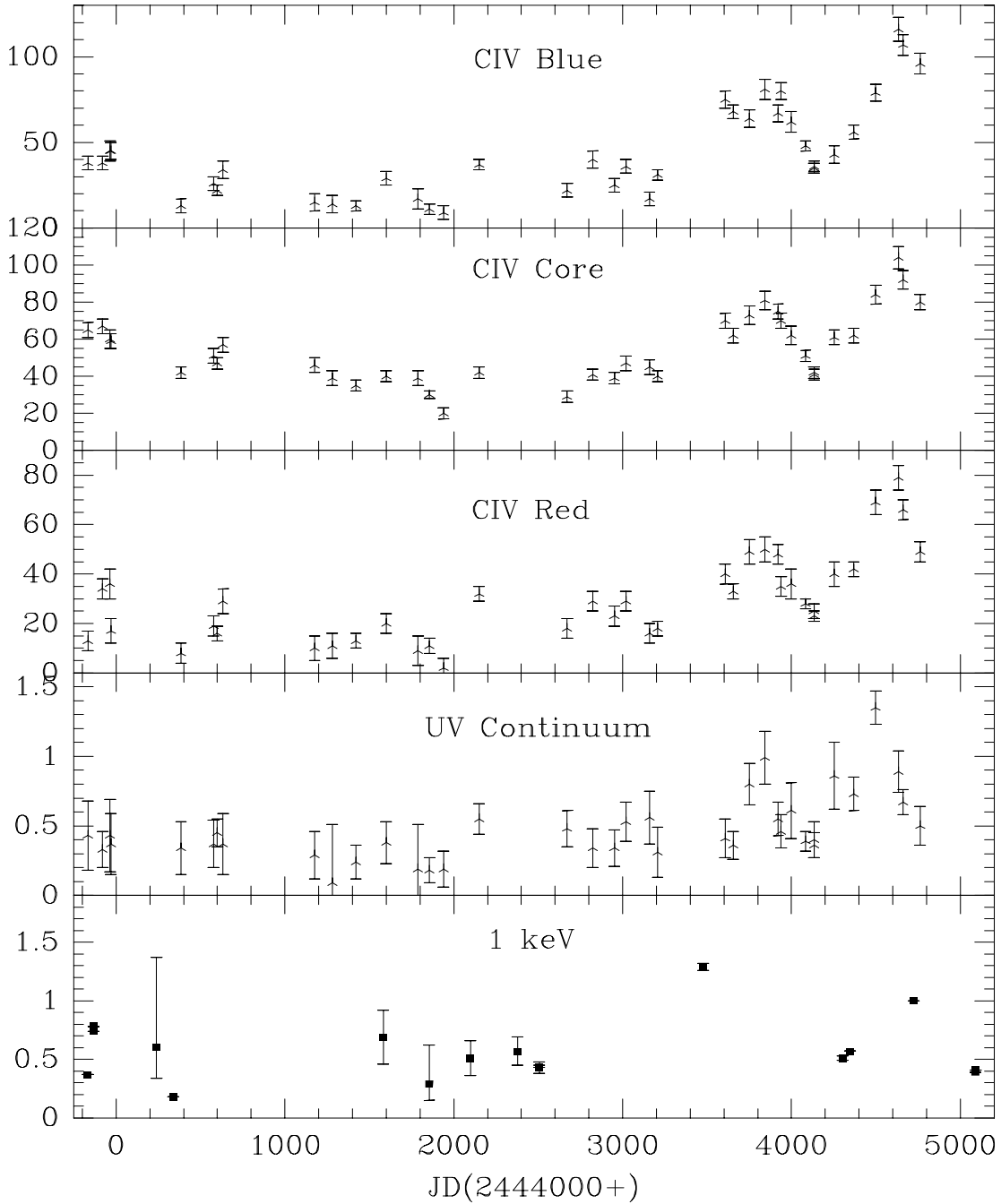


**Figure 1.** The lightcurves of 3C390.3 in the X-ray (Table 3), UV continuum (Table 1) and the CIV line (Table 2). The CIV line is shown here split up in three velocity domains (blue:  $-7000$  to  $-1800$   $\text{km s}^{-1}$ ; core:  $-1800$  to  $+1800$   $\text{km s}^{-1}$  and red:  $+1800$  to  $+7000$   $\text{km s}^{-1}$ ). The X-ray lightcurve shows the presence of a large increase in brightness Nov. 1988 (JD6500). At this time no UV observations were made, but the effects of this event can still be seen in the blue lightcurve of CIV at (JD6600). The fluxes are in the rest frame of 3C390.3 and are in units of  $10^{-14}$   $\text{erg s}^{-1} \text{cm}^{-2} \text{\AA}^{-1}$  for the continuum and  $10^{-14}$   $\text{erg s}^{-1} \text{cm}^{-2}$  for the emission lines.

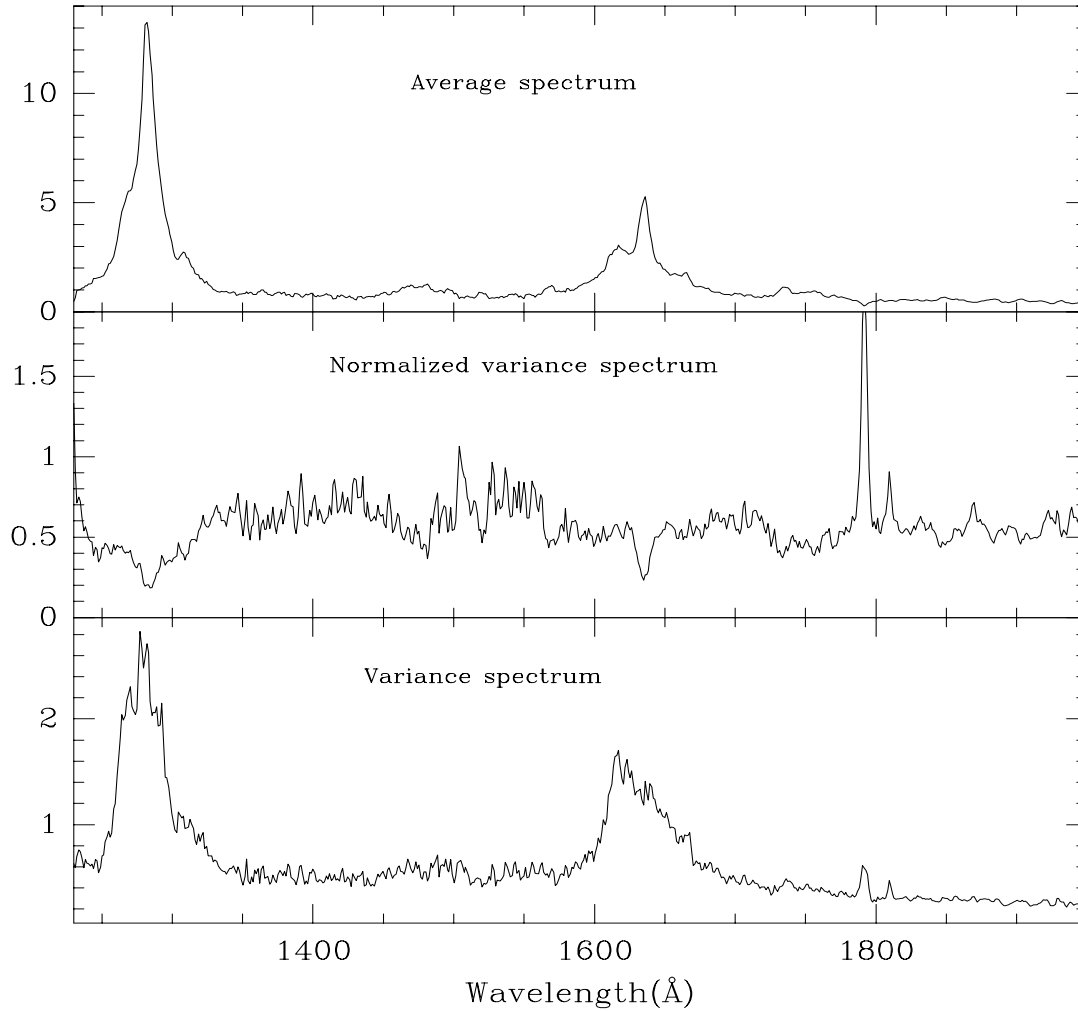


**Figure 2.** The top panel shows the average SWP spectrum of 3C390.3 and the bottom panel shows the variance spectrum (the narrow peaks in the variance near 1800Å are due to a reseau mark in the camera). It is clear that variability exists over the full spectral range. Note the strong asymmetry in the variance spectrum of especially CIV. The middle panel shows the normalized variance spectrum (i.e. the quotient of the bottom spectrum with the top one). The flat-bottomed troughs at the position of  $Ly\alpha$  and CIV show that the amplitude of the variability is quite similar over the full width of the broad lines even though the line shape is quite asymmetric with respect to the systemic velocity.

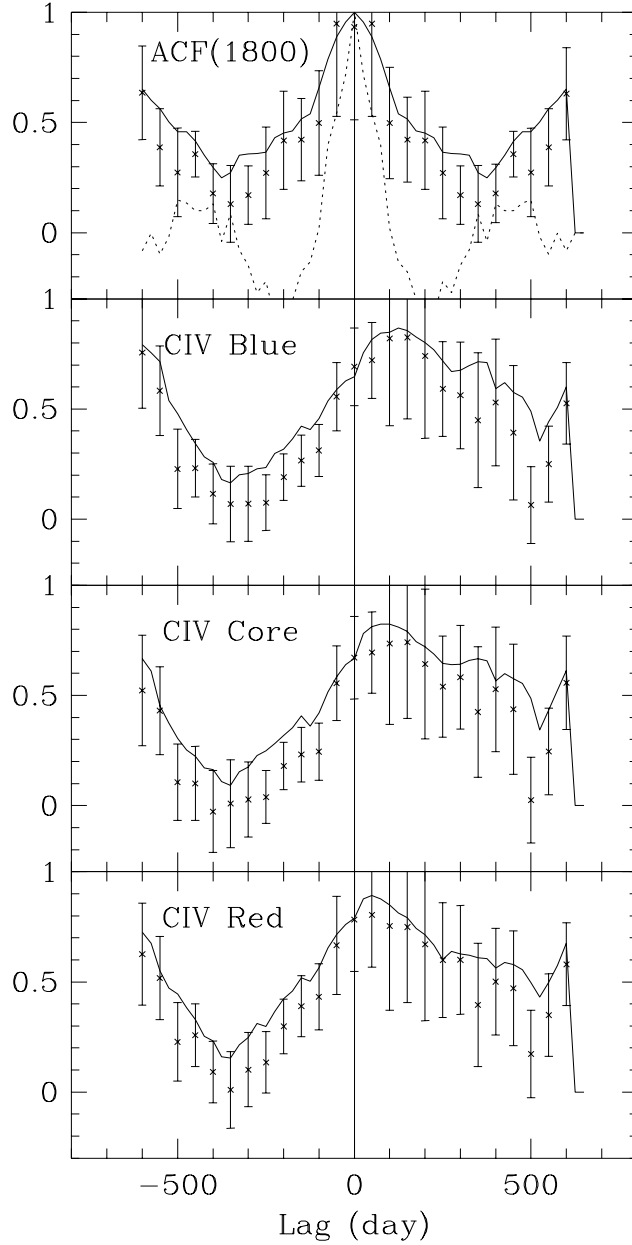


**Figure 3.** From top to bottom this figure shows the ACF at  $1800\text{\AA}$  with the ACF for the sampling window (top), and the CCF for CIV with the continuum in the velocity range chosen (see also Figure 1 and text). All boxes show both the Interpolated cross-correlation (solid curves) and the discrete correlation functions (with error bars). The sampling window autocorrelation function is shown dashed in the top panel. For reference the vertical line in the figure shows the position associated with no delay in the line response. The difference in the delay between the red and blue sides of the line can be easily discerned and is also present in the direct CCF between the red and blue sides of the line. The correlation functions for  $L\gamma\alpha$  are very similar to those of CIV (see also Table 5).

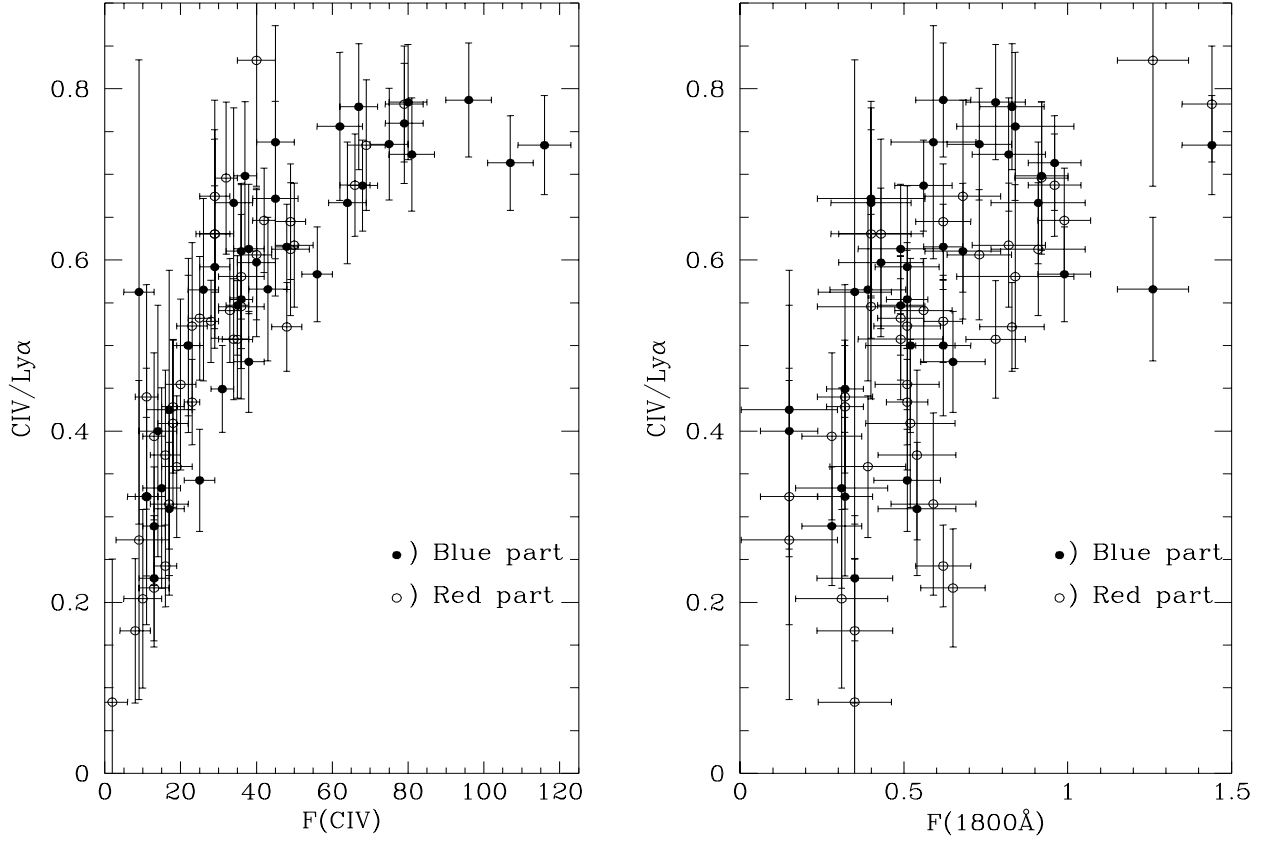


**Figure 4.** This figure shows on the right-hand side the relation between the  $CIV/Ly\alpha$  ratio and the continuum and on the left-hand side with the  $CIV$  intensity itself, for both the blue wing (filled symbols) and the red wing (open symbols). Note that the scatter in the left diagram is much less than in the continuum diagram on the right. This is predominantly due to the fact that time delay effects are absent in the left-hand diagram. Note also that the  $CIV/Ly\alpha$  rises steeply with the continuum as measured by the  $CIV$  flux, but appears to remain constant above  $I_{CIV} > 60$  (corresponding to  $F_{1800\text{\AA}} > 0.6 \cdot 10^{-14} \text{ erg s}^{-1} \text{ cm}^{-2} \text{ \AA}^{-1}$ ). This is a strong indication of a mixed population of optically thin and optically thick BLR clouds. The fluxes are in the rest frame of 3C390.3 and are in units of  $10^{-14} \text{ erg s}^{-1} \text{ cm}^{-2} \text{ \AA}^{-1}$  for the continuum and  $10^{-14} \text{ erg s}^{-1} \text{ cm}^{-2}$  for the emission lines.

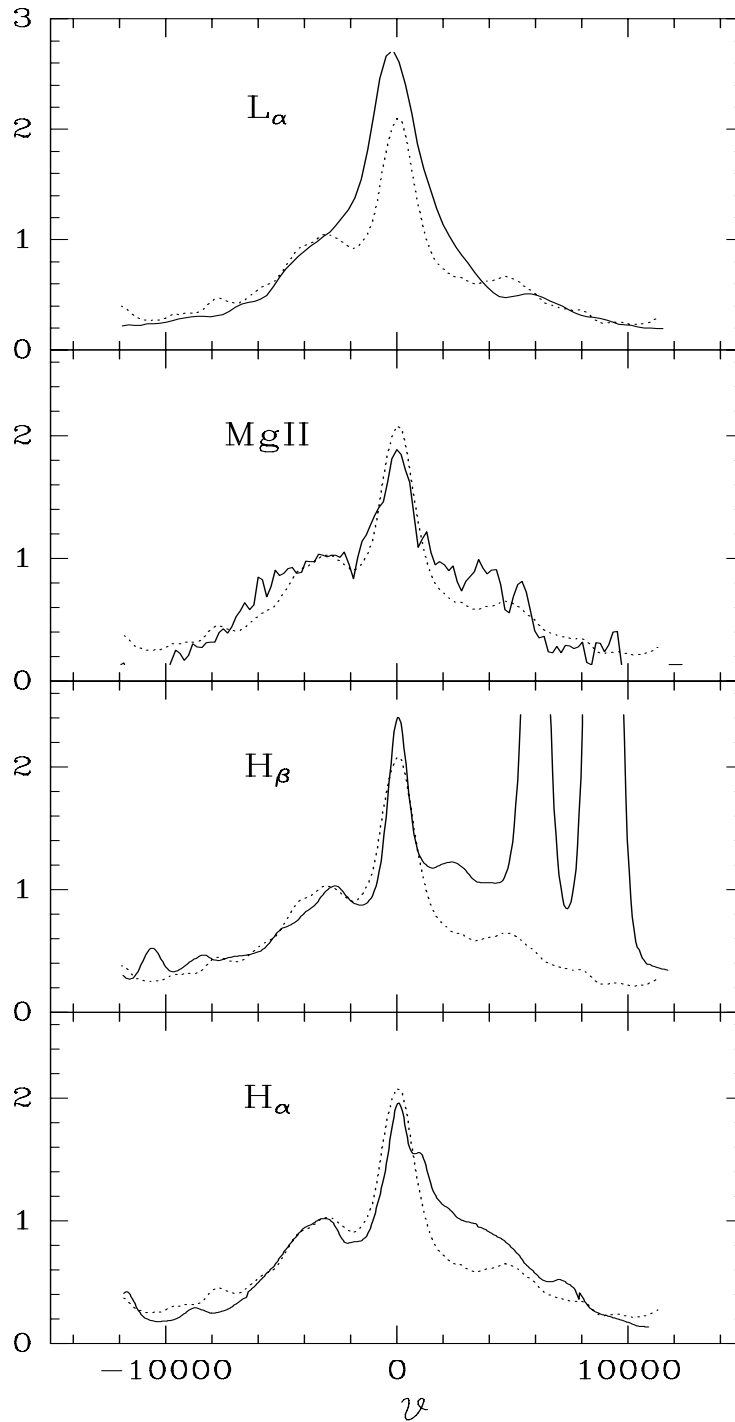


**Figure 5.** Average line profiles over the period 1978–1991 for the UV lines and 1975–1988 for the optical lines. We show the profiles of  $Ly\alpha$ , CIV, MgII,  $H\beta$  and  $H\alpha$ . The CIV line profile is shown as a dotted line. This diagram clearly illustrates the difference between the Balmer lines and the UV lines. Both  $H\alpha$  and  $H\beta$  show a strong red peak. This is the part of the Balmer lines which does not respond to the UV continuum variations and is therefore not associated with the BLR (see also Veilleux and Zheng, 1991).



**Figure 6. (not included)** This figure shows schematically the observed configuration of the BLR of 3C390.3. The angles indicated, are the angles with respect to the line-of-sight (l.o.s.) determined from the observed superluminal motion and from the observed delays between the red and blue side of the UV lines. Since these angles correspond with those derived from the accretion disk model fit for the wings of  $H\alpha$  by Eracleous and Halpern (1994), and the UV lines suggest a strong rotational, infalling velocity field, these independent results are only consistent, if the UV lines from the BLR are associated with an accretion disk as indicated.